Supplementary information for

Linking the scaling of tremor and slow slip near Parkfield, CA

Hui Huang[1*] and Jessica C. Hawthorne[1]

[1]*Department of Earth Sciences, University of Oxford, Oxford, UK*

[*]*Correspondence to: oldyellow9451@gmail.com*

Contents of this file

Text S1, Figs. S1-S28, Dataset S1

Text S1

Mapping moment ratios to amplitude ratios while accounting for detection bias

The peak amplitude of an LFE with the same moment decays approximately as the inverse of duration (Fig. S20). Therefore the detection capability of a longer LFE with the same moment decreases. To understand this effect on observed moment-duration scalings, we generate synthetic LFE waveforms with different moments and durations. The moments of synthetic events are relative to the average LFE at 0.2 sec, which is corresponding to the stacked 0.2-sec detection waveforms and assumed to have a moment of 1. Based on the moment-amplitude-duration relation (Fig. S20), synthetic waveforms with different moments (10^{-4}-10^{4}) and durations (0.1-0.6 sec) are generated with amplitudes scaled relative to the 0.2-sec event stack. Then we add noises randomly extracted from real data to the synthetic waveforms. We cross correlate and stack all synthetic events with different-duration templates. The detection threshold is set as the same as that used in the matched-filter detection. When an event is detected, it is marked as a symbol in Fig. S21a. The result shows that the lower bound of detections' moment increases with duration, consistent with expectations. Then we count the number of detections for each duration and calculate the percentage of detection using moving windows along the moment axis. This results in the detection probabilities of moment for all durations (Fig. S21b).

We multiply the detection probabilities by the corresponding input moment distributions at different durations. We consider three cases: linear moment duration scaling ($M_0 \propto T$), moment duration cubed scaling ($M_0 \propto T^3$) and moment independent of duration scaling (moment equals constant, $M_0 = C$). The real mean moment for a 0.2-sec event may be slightly lower than the 0.2-sec event stack (with moment of 1). To test this effect, we set the 0.2-sec mean moment as 1, 0.5, 0.1 and 0.01. We generate a series of moment distributions (log-normal with σ of 0.5), with the mean moment varying by different moment-duration scaling relations (Figs. S22-S25). All distributions are multiplied by corresponding detection probabilities to obtain the corrected observed moment distributions. Then 1000 random samples are drawn from the corrected distributions and the mean values represent the expected moment after accounting for detection bias. Note that if the reference moment is 1 or 0.5, the input scaling relations of all three cases can be correctly recovered (Figs. S22 and S23). If the 0.2-sec mean moment is 0.1 or even lower (0.01), the recovered scalings for $M_0 \propto T^3$ and $M_0 = C$ start to be biased towards $M_0 \propto T$ (Figs. S24 and S25). The expected moments are converted back to amplitudes based on the amplitude-moment relation (Fig. S20). The median, 5 and 95 percent of the 1000 realizations are obtained and compared to observations. As shown in Figs. 4 and S26-S28, the observations are uniquely consistent with $M_0 \propto T$ when the 0.2-sec mean moment is from 1, 0.5 down to 0.1, but indistinguishable between $M_0 \propto T$ and $M_0 = C$ if the 0.2-sec mean moment is 0.01 (Fig. S28). We consider that the real 0.2-sec mean moment is close to 1, which means that the amplitude of the 0.2-sec stack is close to the real value. In the main text, we show the scaling predictions with the 0.2-sec mean moment equal to 1 (Fig. 4).

Effect of moment or duration binning on scaling

We add a note here that binning the LFE measurements by moment or duration may sometimes lead to bias in scaling, given the uncertainties of measurements. Here we add one extra analysis of the dataset produced by Supino et al. (2020), for LFEs in the Nankai subduction zone. We find that binning by moment can lead to a scaling close to $M_0 \propto T$ while binning by duration leads to a $M_0 \propto T^3$ scaling (Fig. S15). To understand this binning effect, we carry out two synthetic datasets by generating data points of moments and corner frequencies, following $M_0 \propto T$ or $M_0 \propto T^3$ scaling relations. For the $M_0 \propto T$ dataset (Fig. S16), we fix the corner frequencies but add some random errors to the moments (Fig. S17). In contrast, for the $M_0 \propto T^3$ dataset (Fig. S18), we fix the moments but add some random errors to the corner frequencies (Fig. S19). We find that for both cases, binning by moment and duration result in different scalings. This illustrates that when large data uncertainties exist, binning inappropriately can sometimes lead to bias in scaling.

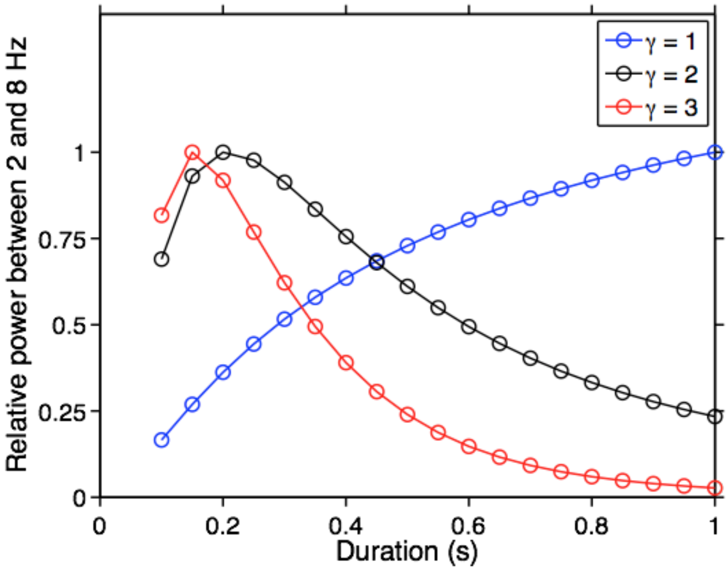

Figure S1. The relative mean velocity spectral power between 2 and 8 Hz band, for LFEs with different durations (0.1 - 1 sec) that follow a linear moment-duration scaling (see also Figs. 1b and 1c). For a fall-off rate γ = 1 (Ide et al., 2007), longer events have larger relative power within 2-8 Hz. For fall-off rates γ >= 2 (Zhang et al., 2011; Supino et al., 2020), the peak occurs at 0.2 sec, suggesting that 0.2-sec duration events have the highest energy within the 2 and 8 Hz band.

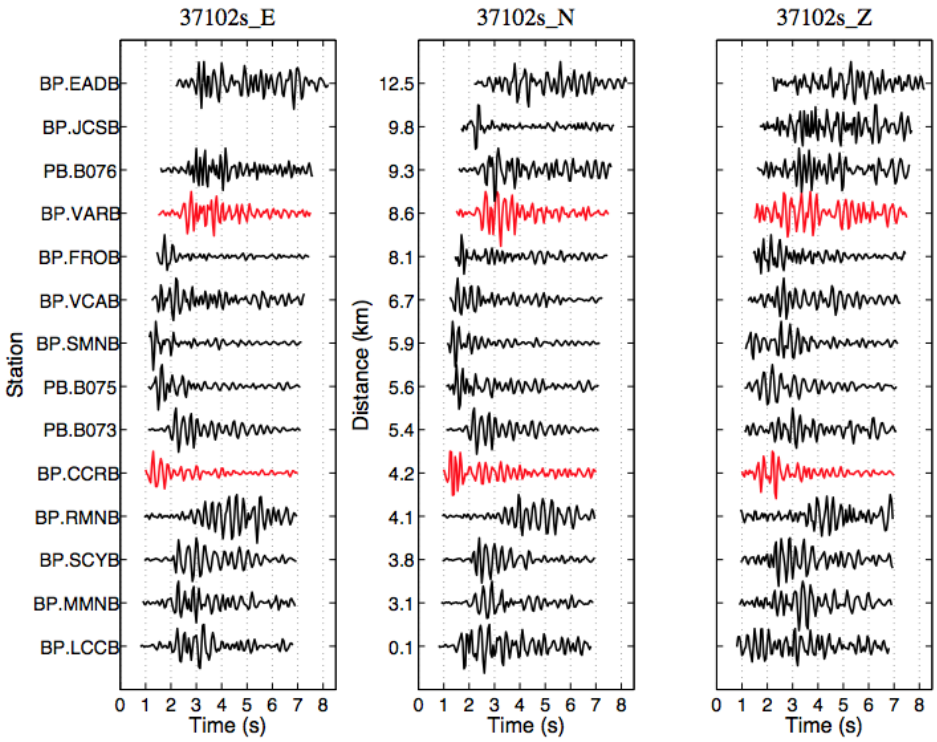

Figure S2. The original template waveforms (family 37102) at all components and stations. Red waveforms denote the two stations which are not used in the detection but reserved for validation (see also main text).

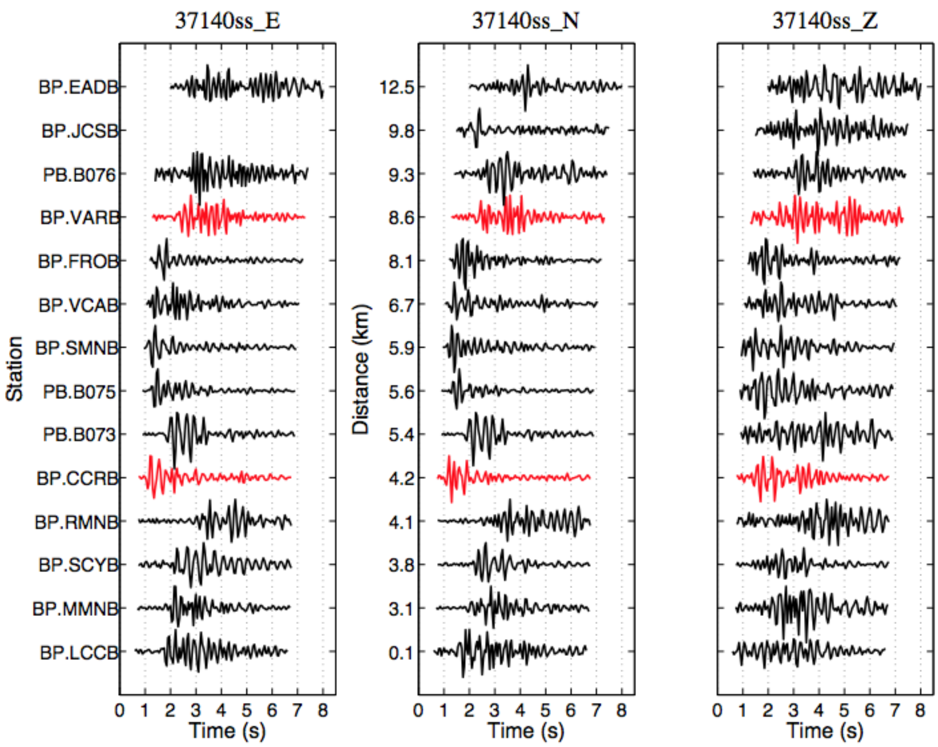

Figure S3. Same as Fig. S2 but for family 37140.

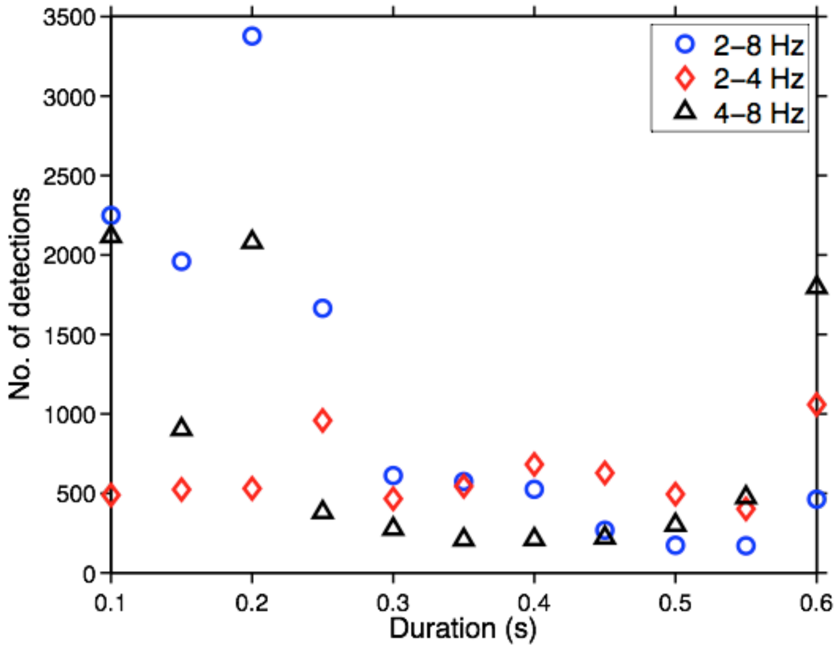

Figure S4. The number of detections at different durations under three frequency bands: 2-8 Hz (blue circles), 2-4 Hz (red diamonds) and 4-8 Hz (black triangles).

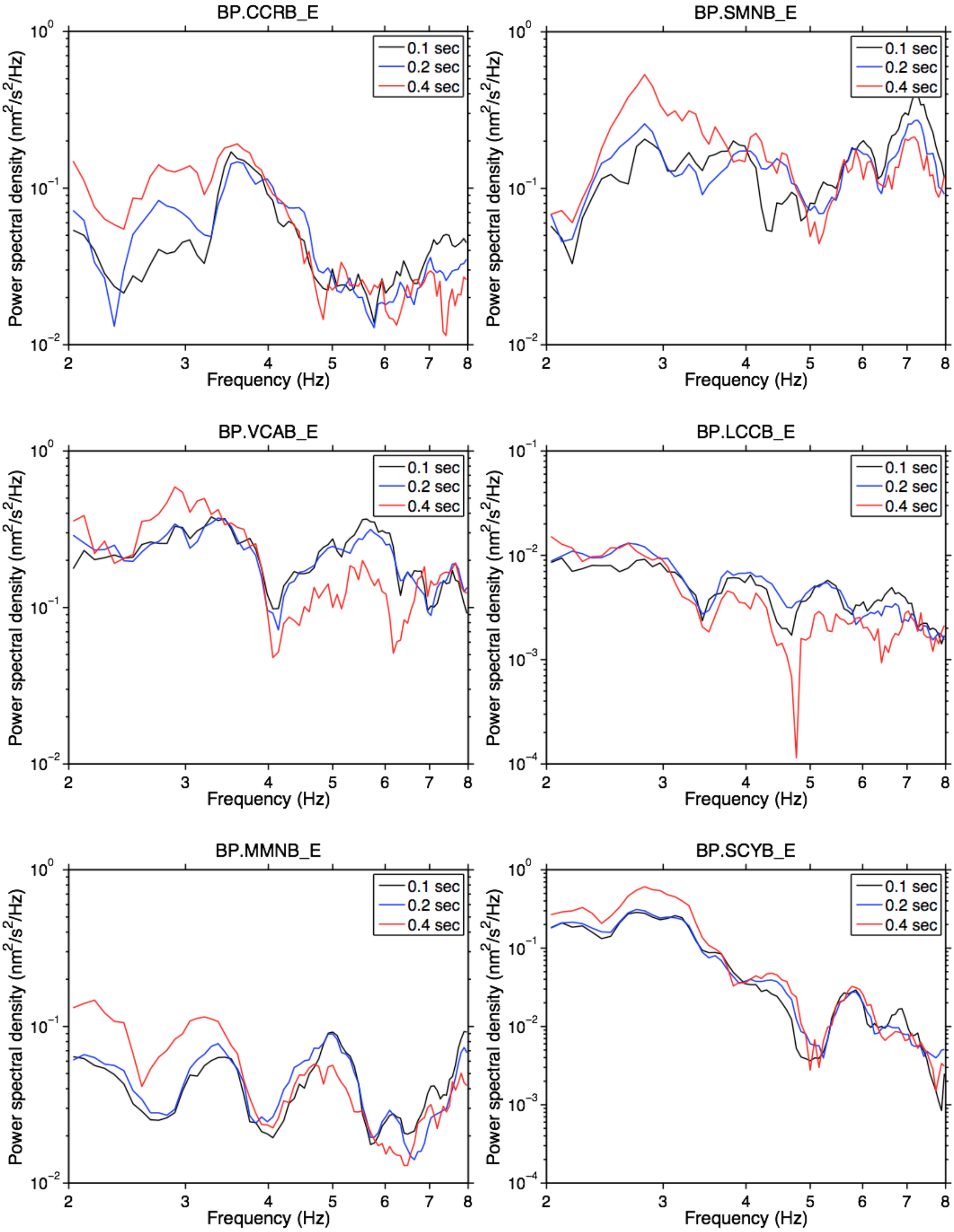

Figure S5. Median velocity spectral power for all detection waveforms (family 37102) at different durations: 0.1 sec (black), 0.2 sec (blue) and 0.4 sec (red). The corresponding noise powers (Fig. S6) have been subtracted from the spectral powers of detection windows. Powers are calculated with multi-taper methods with three tapers ($NW = 2$).

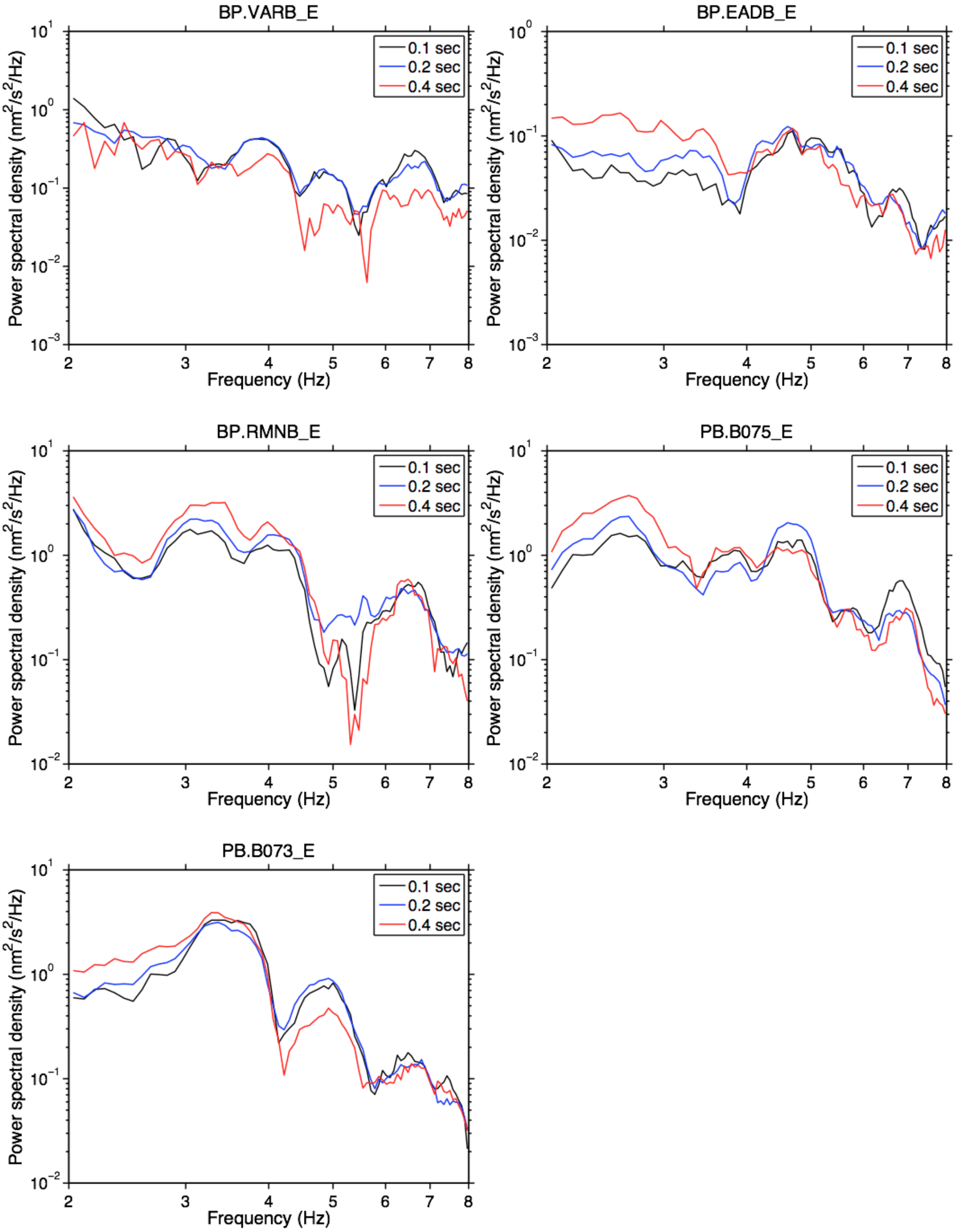

Figure S5 (Continued).

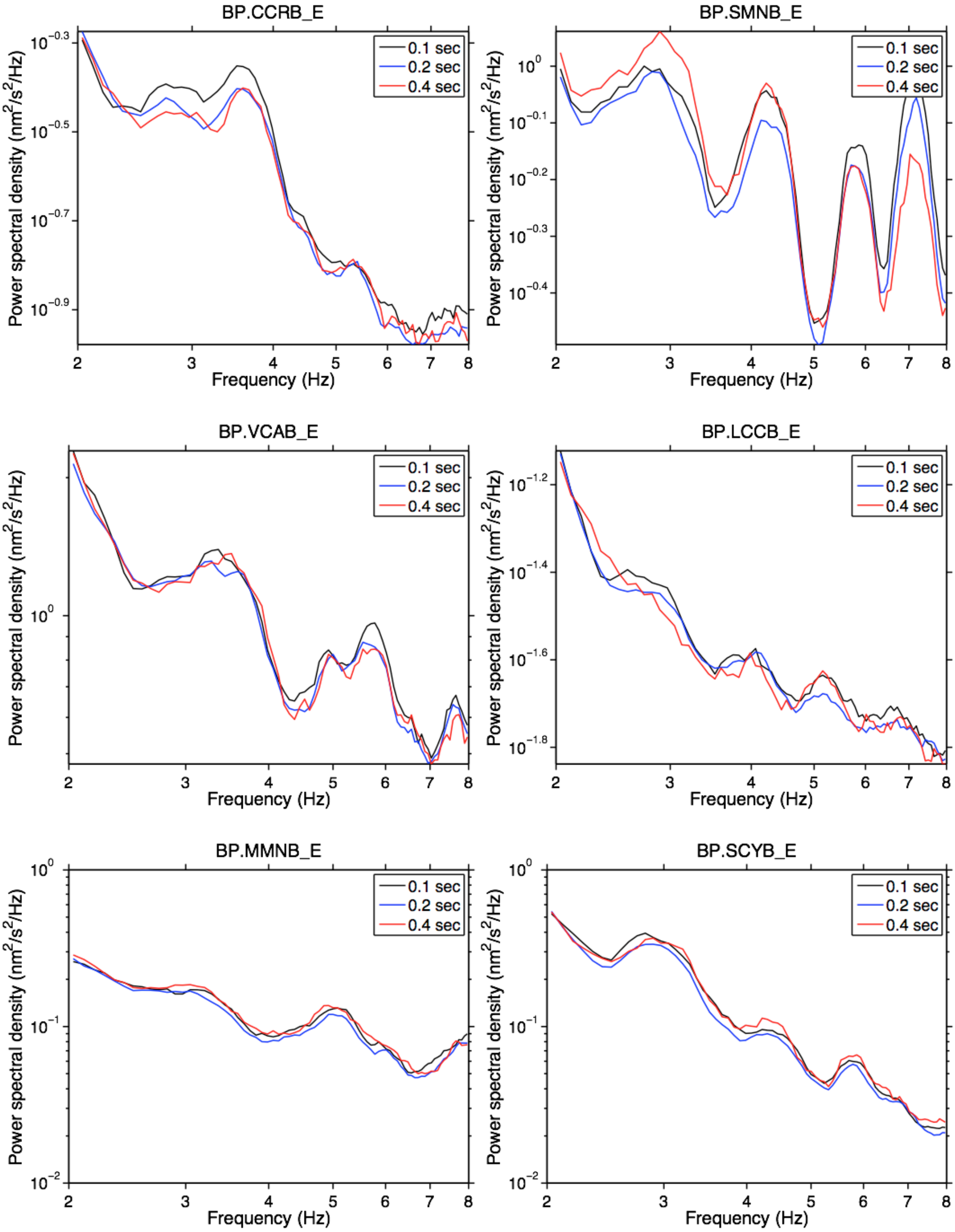

Figure S6. Similar to Fig. S5 but showing the median noise powers measured on the noise windows 2 sec before the corresponding detection windows (family 37102).

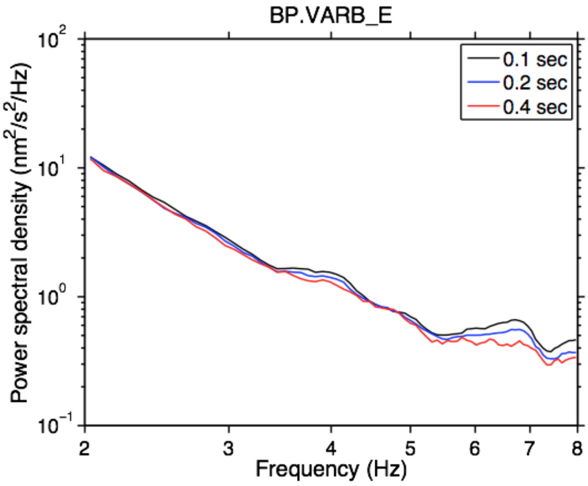

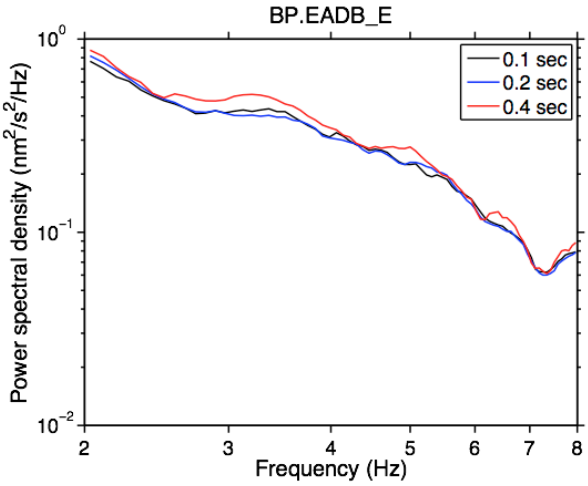

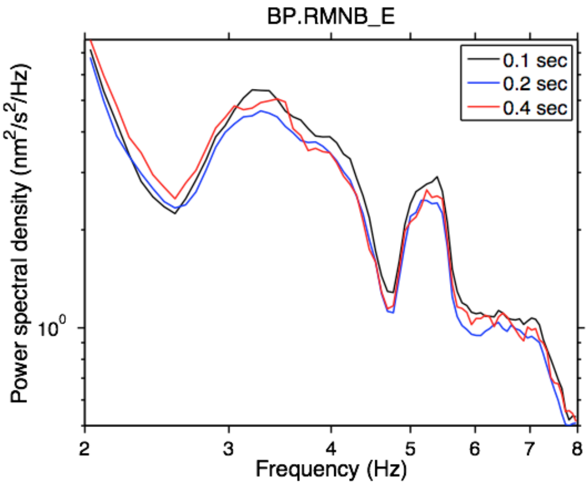

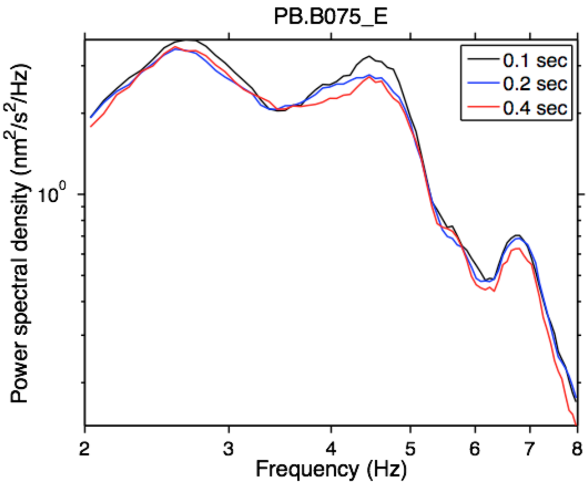

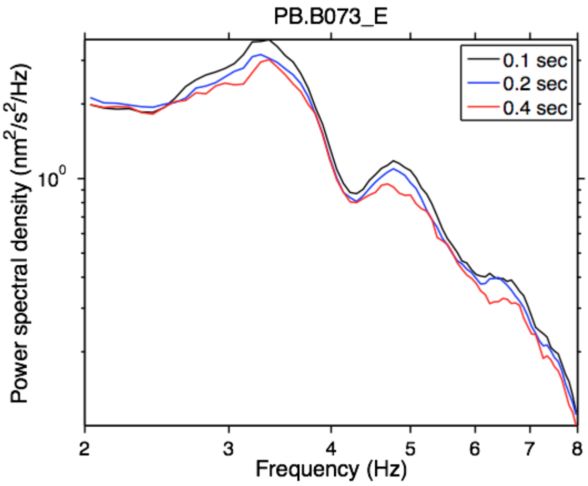

Figure S6 (Continued).

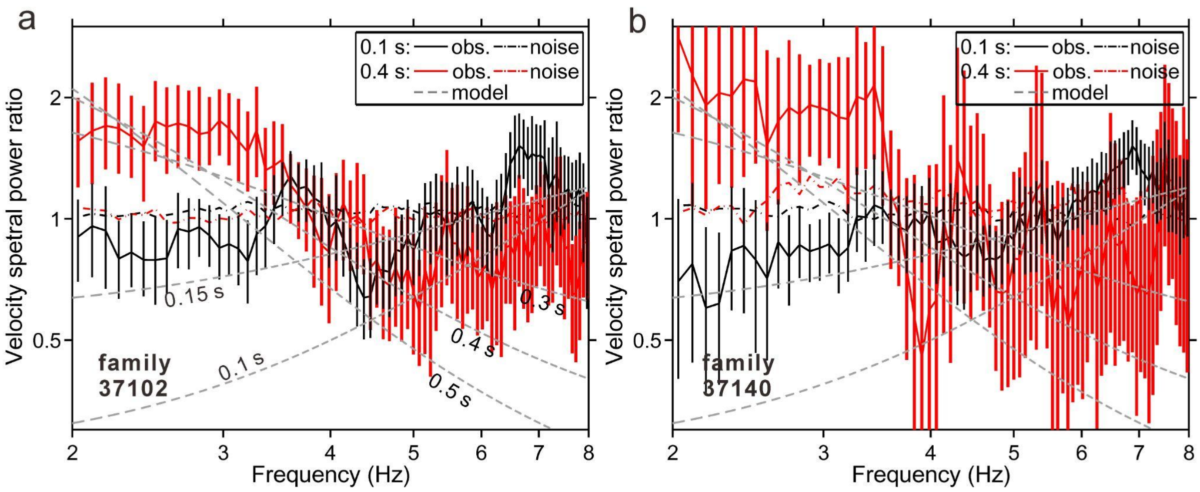

Figure S7. The power ratio uncertainties (Figs. 4a and 4b) from bootstrapping the individual spectra. The 0.1-sec and 0.4-sec spectra are separated at low frequencies (2-3.5 Hz) and high frequencies (6-7 Hz).

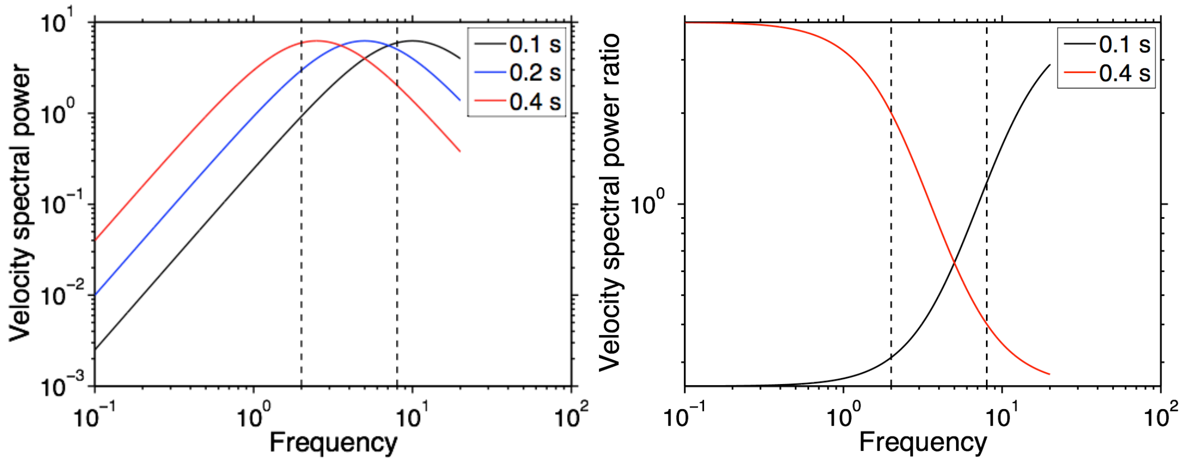

Figure S8. The theoretical velocity spectral power and power ratios assuming a linear moment-duration scaling and γ = 2. The left figure is the same as Fig. 1b.

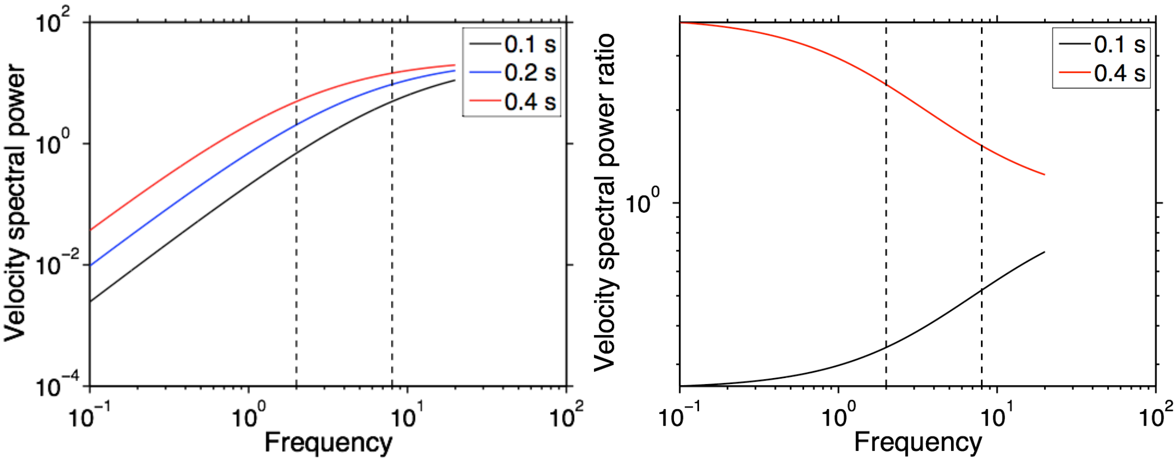

Figure S9. Theoretical velocity spectral power and power ratios assuming a linear moment duration scaling and $\gamma = 1$.

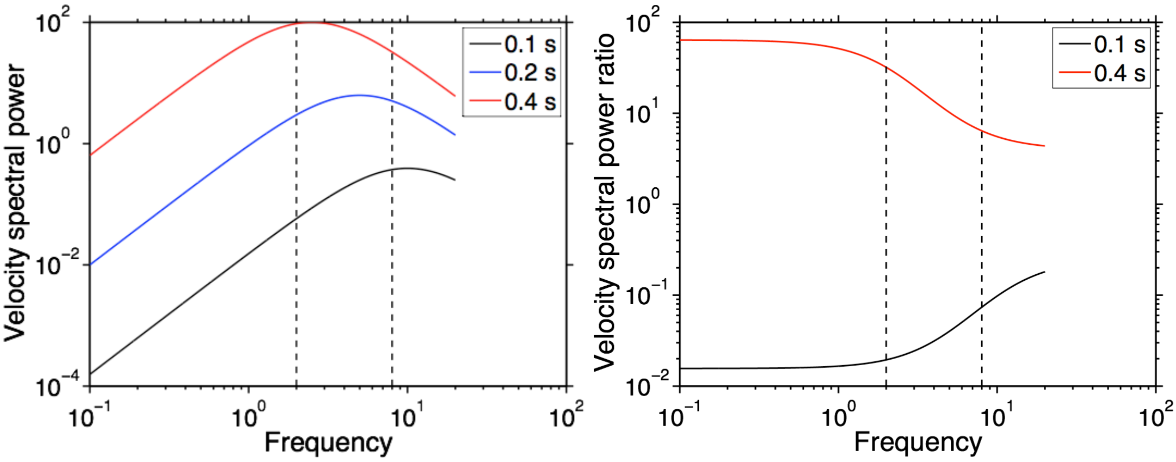

Figure S10. Theoretical velocity power and power ratios assuming a moment duration cubed scaling and $\gamma = 2$.

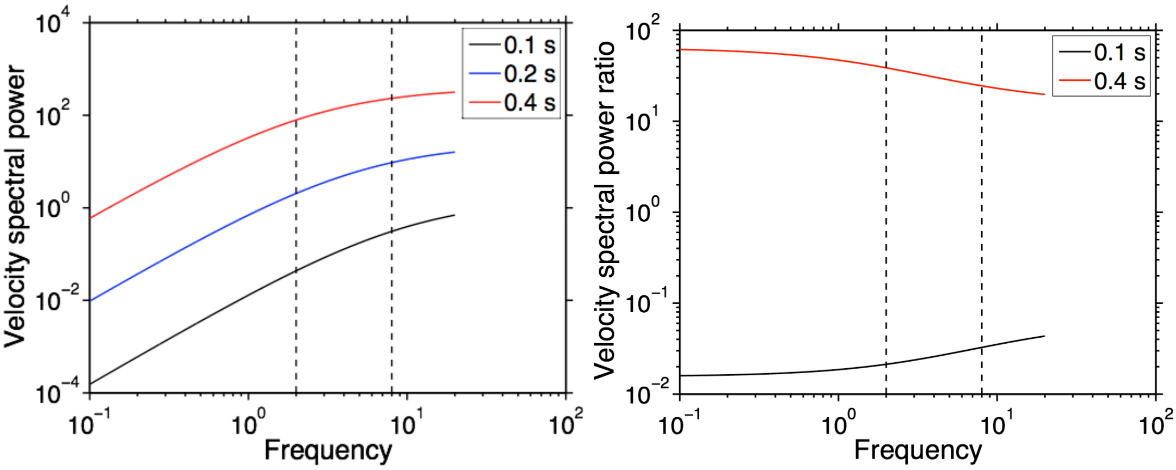

Figure S11. Theoretical velocity power and power ratios assuming a moment duration cubed scaling and $\gamma = 1$.

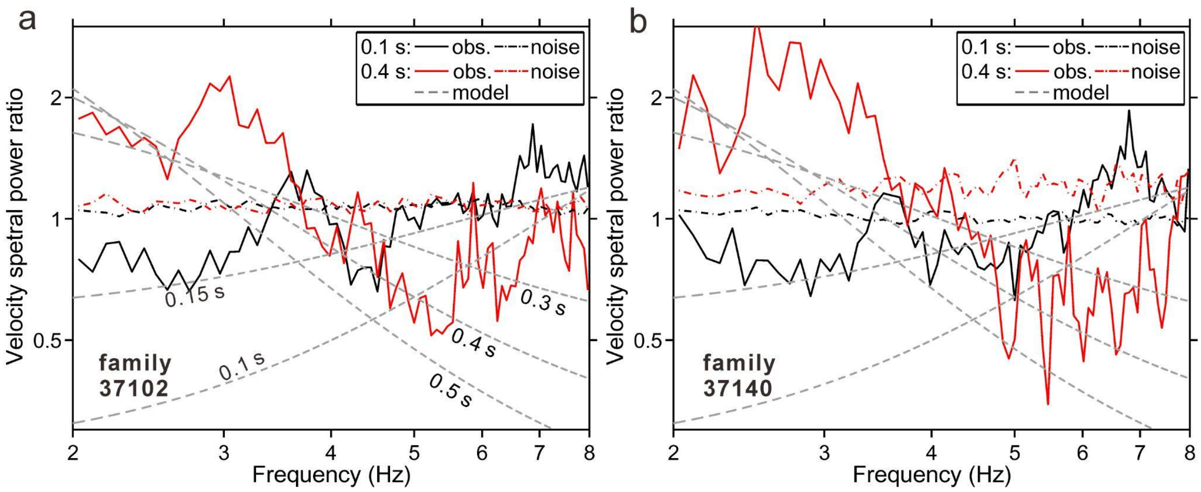

Figure S12. Similar to Figs. 4a-4b in the main text but for the other horizontal component (channel code: 3) for families 37102 and 37140.

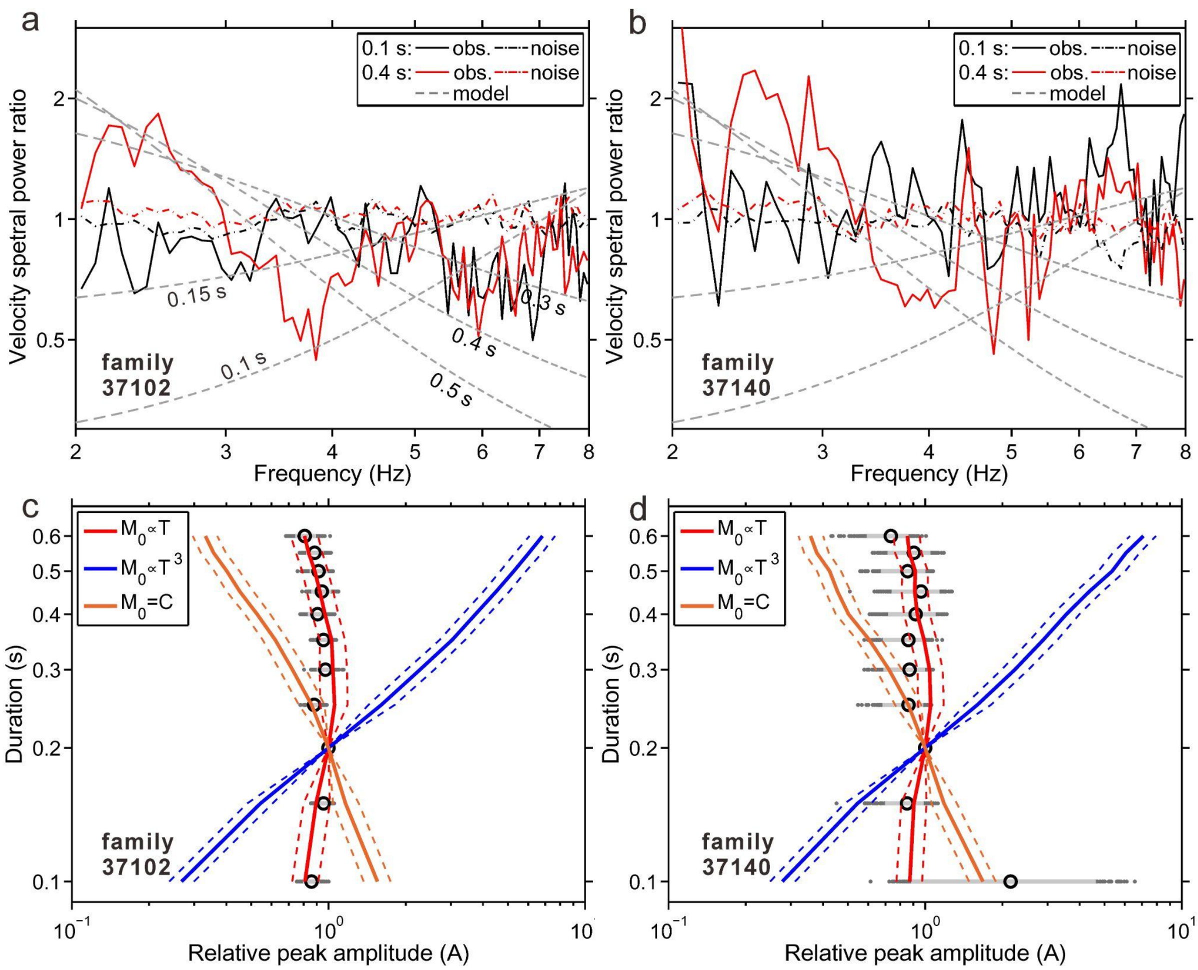

Figure S13. Same as Fig. 4 in the main text but for the catalog of LFEs detected and classified in the 2-4 Hz band.

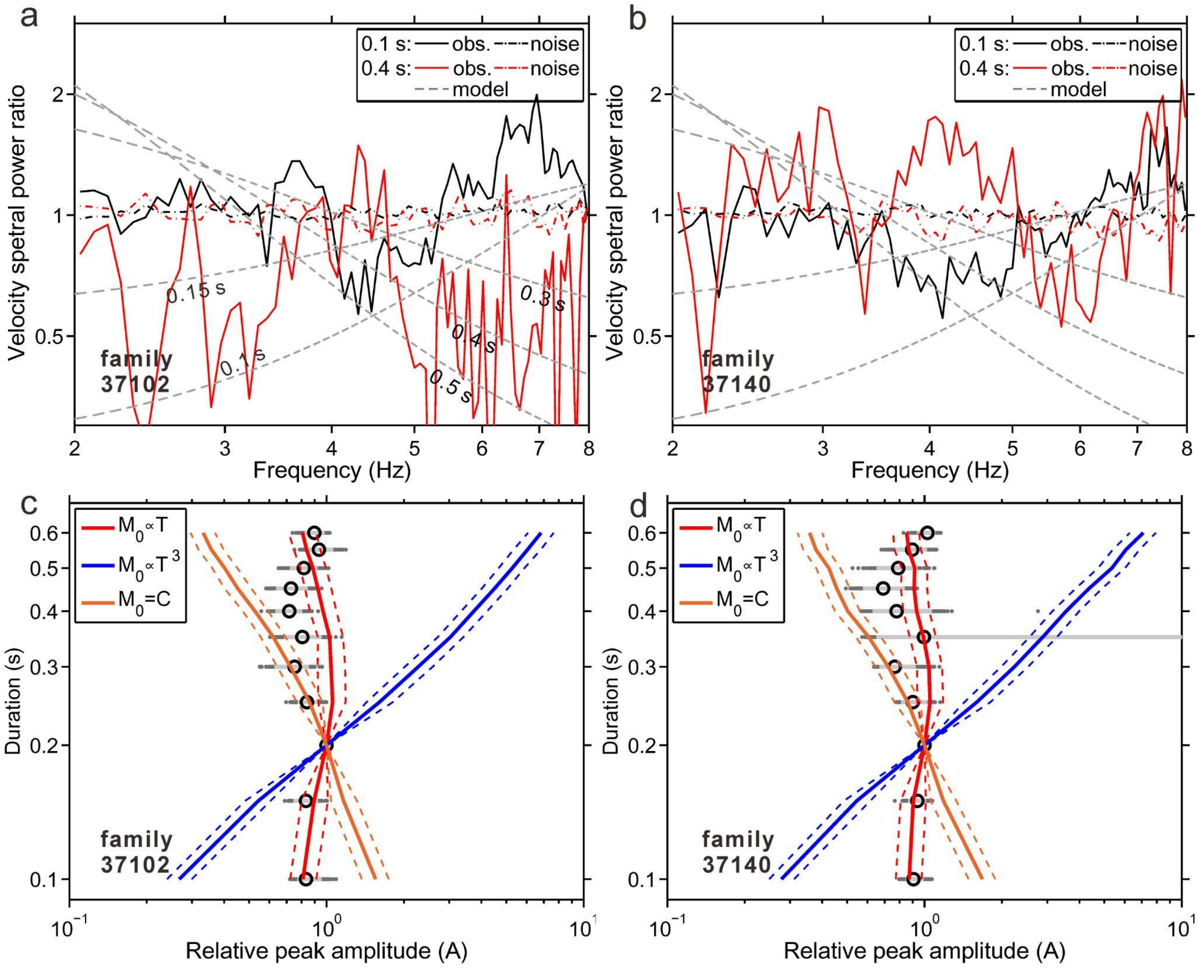

Figure S14. Same as Fig. 4 in the main text but for the catalog of LFEs detected and classified in the 4-8 Hz band.

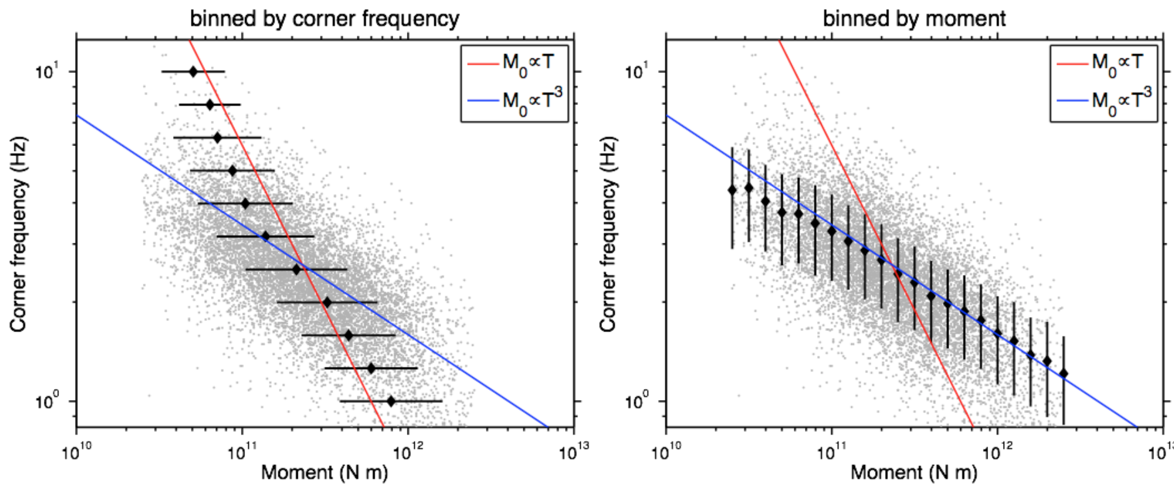

Figure S15. Different scaling results when binning observations by corner frequency (left) and moment (right), using the data produced by Supino et al. (2020).

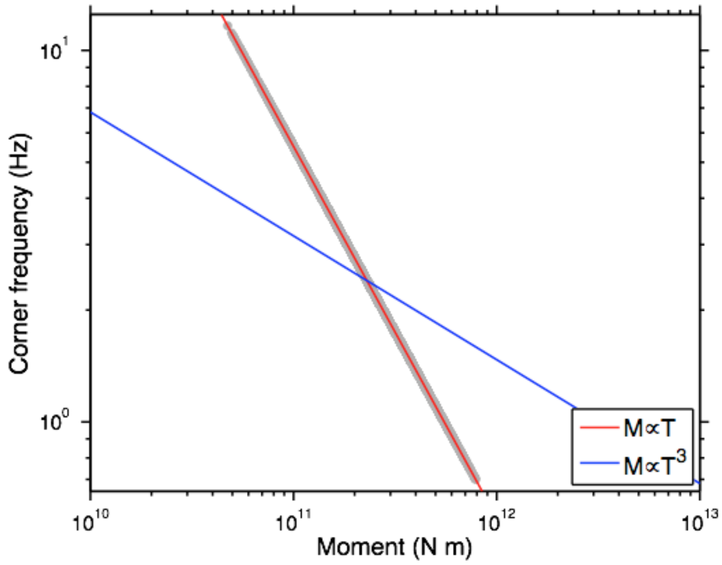

Figure S16. Synthetic data points (gray dots) following a linear moment-duration scaling (red line).

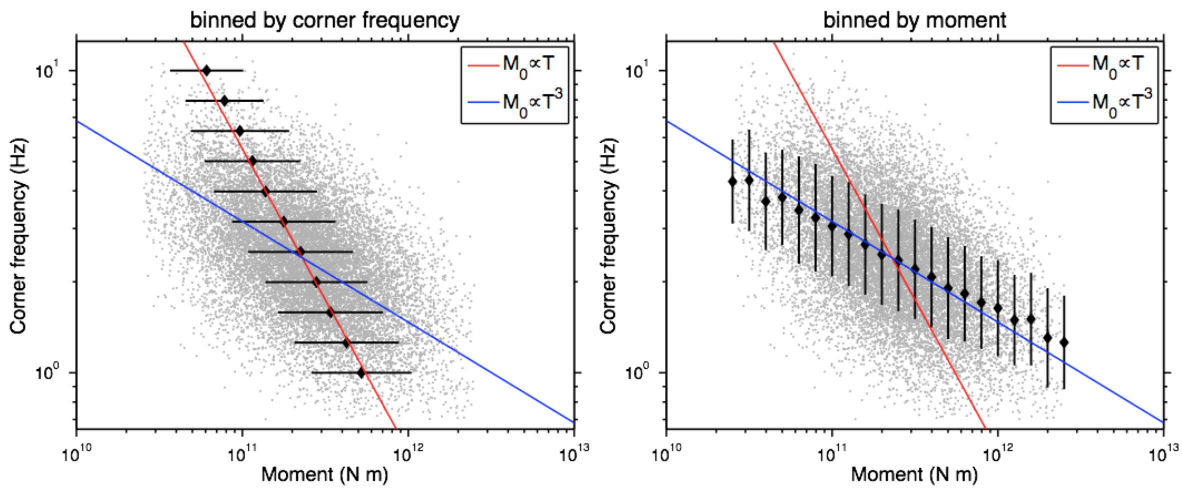

Figure S17. Synthetic data from Fig. S16 are randomly perturbed along the moment axis, while the corner frequencies of the data points are unchanged. Note that binning by corner frequency (left) recovers the correct input scaling (Fig. S16) while binning by moment does not.

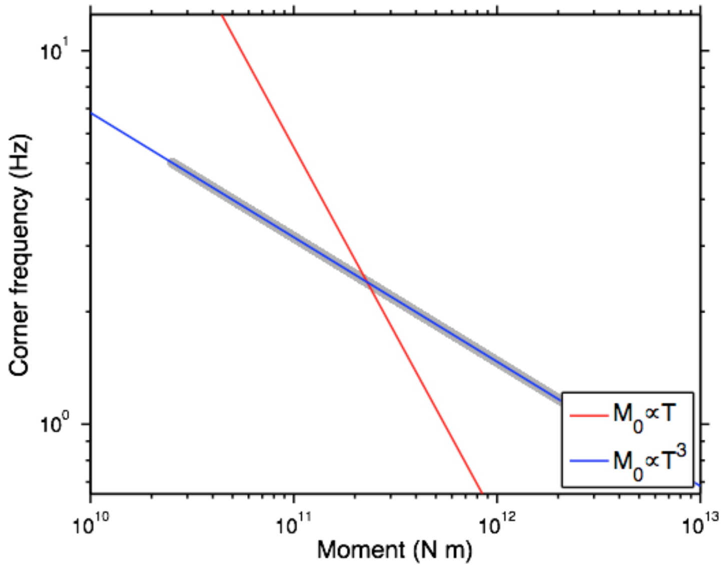

Figure S18. Synthetic data points (gray dots) following a moment duration cubed scaling (blue line).

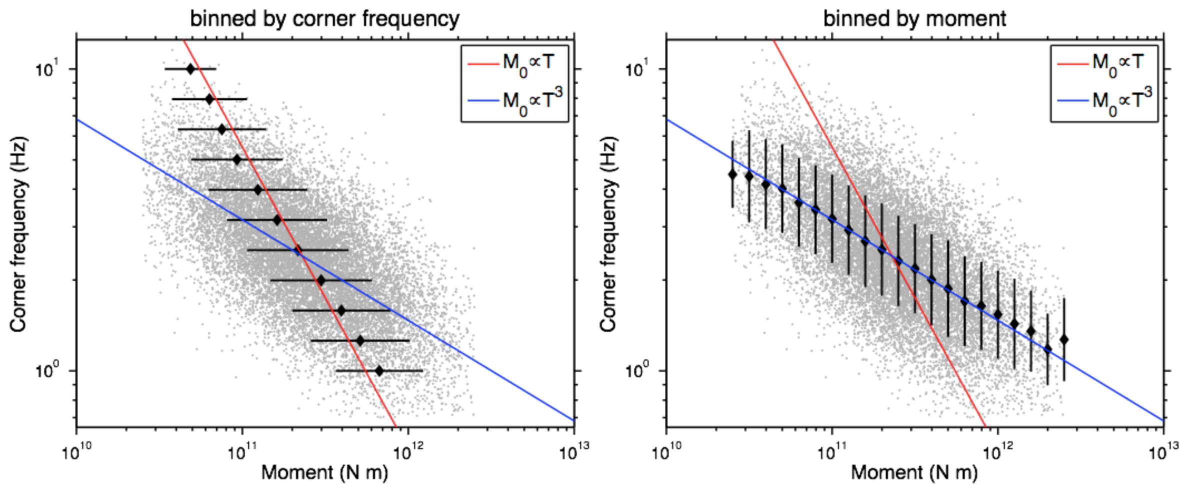

Figure S19. Synthetic data from Fig. S18 are randomly perturbed along the corner frequency axis, while the moments of the data points are unchanged. Note that binning by moment (right) recovers the correct input scaling (Fig. S18) while binning by corner frequency (left) does not.

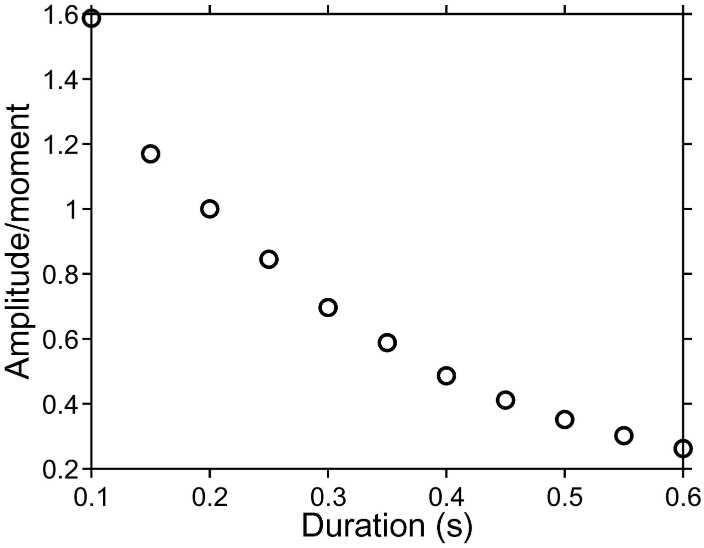

Figure S20. The variation of amplitude/moment ratio with duration, estimated from synthetic templates with normalized moments at different durations.

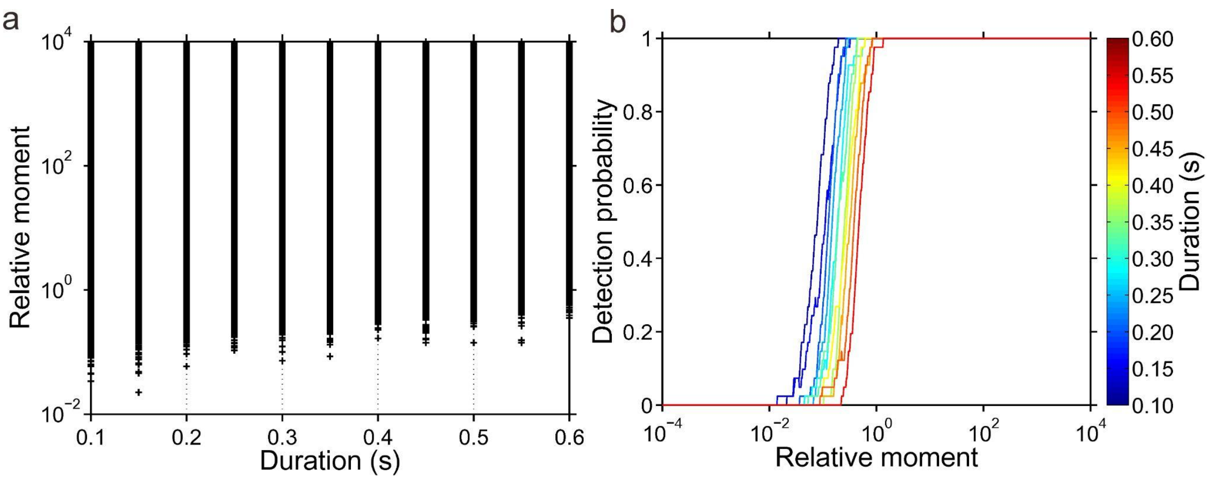

Figure S21. Variation of detection capabilities of LFEs with different durations. (a). Symbols mark the synthetic events that can be detected under the same threshold used in the matched-filter detection. The moment for linearly stacked 0.2-sec detection waveforms is set as 1 and moments of all other events are relative to that (see Text S1 for details). (b). The curves show the detection probabilities for different durations, converted from the data shown in (a). The leftmost curve corresponds to 0.1 sec while the rightmost corresponds to 0.6 sec.

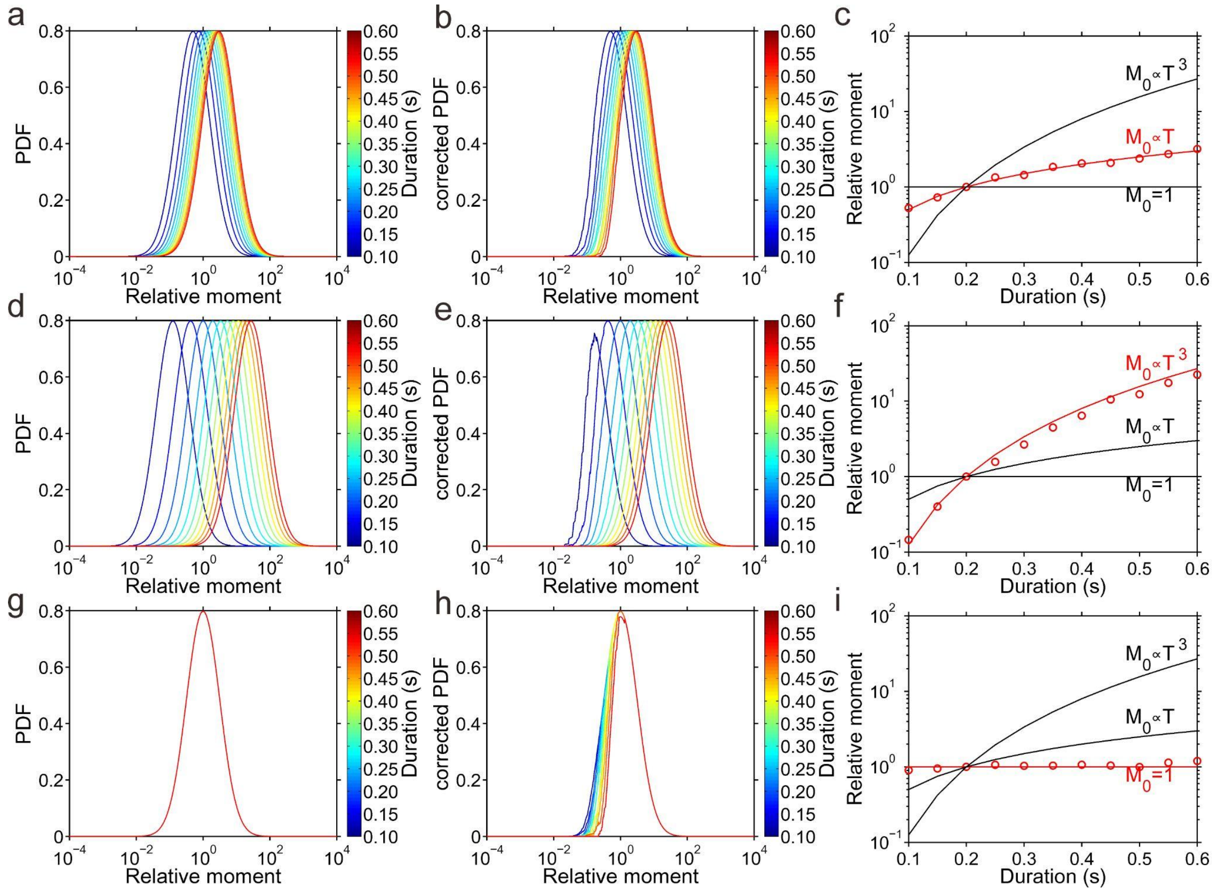

Figure S22. Synthetic tests showing the effect of varying detection capabilities on the estimation of moment duration scaling. Three input moment distributions are considered: linear moment duration scaling (a), moment duration cubed (d) and constant moment (g). In each case, moment distributions have their mean moments scaling with durations (0.1 - 0.6 sec) differently. (b), (e) and (h) show the corrected distributions which are the product of the moment distributions with the corresponding detection probabilities (Fig. S21b). (c), (f) and (i) show the output moment-duration relations (red dots), which are realizations of the corrected moment distributions. The input moment-duration scaling relations are shown in red lines. Note that in this test, the relative moment at 0.2 sec is set to 1.

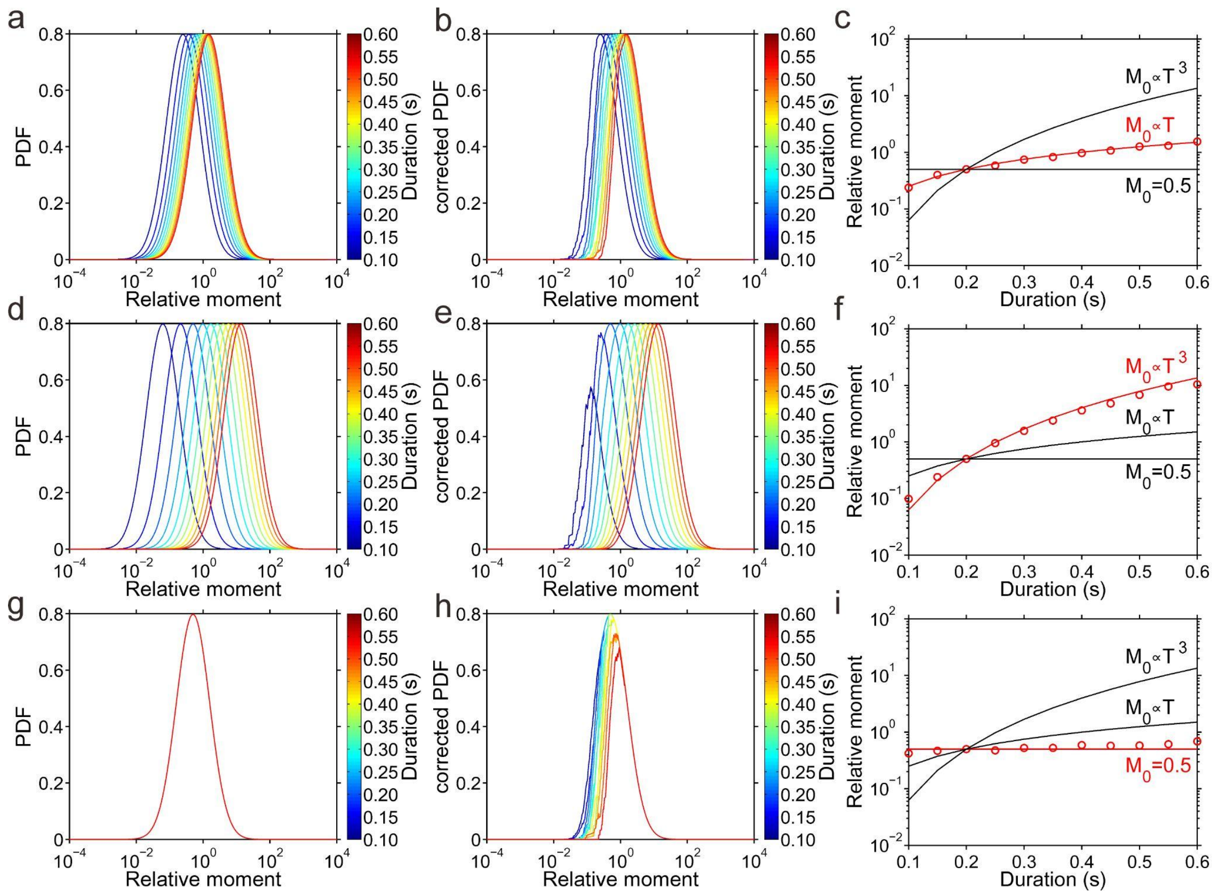

Figure S23. Same as Fig. S22 except that the relative moment at 0.2 sec is set to 0.5.

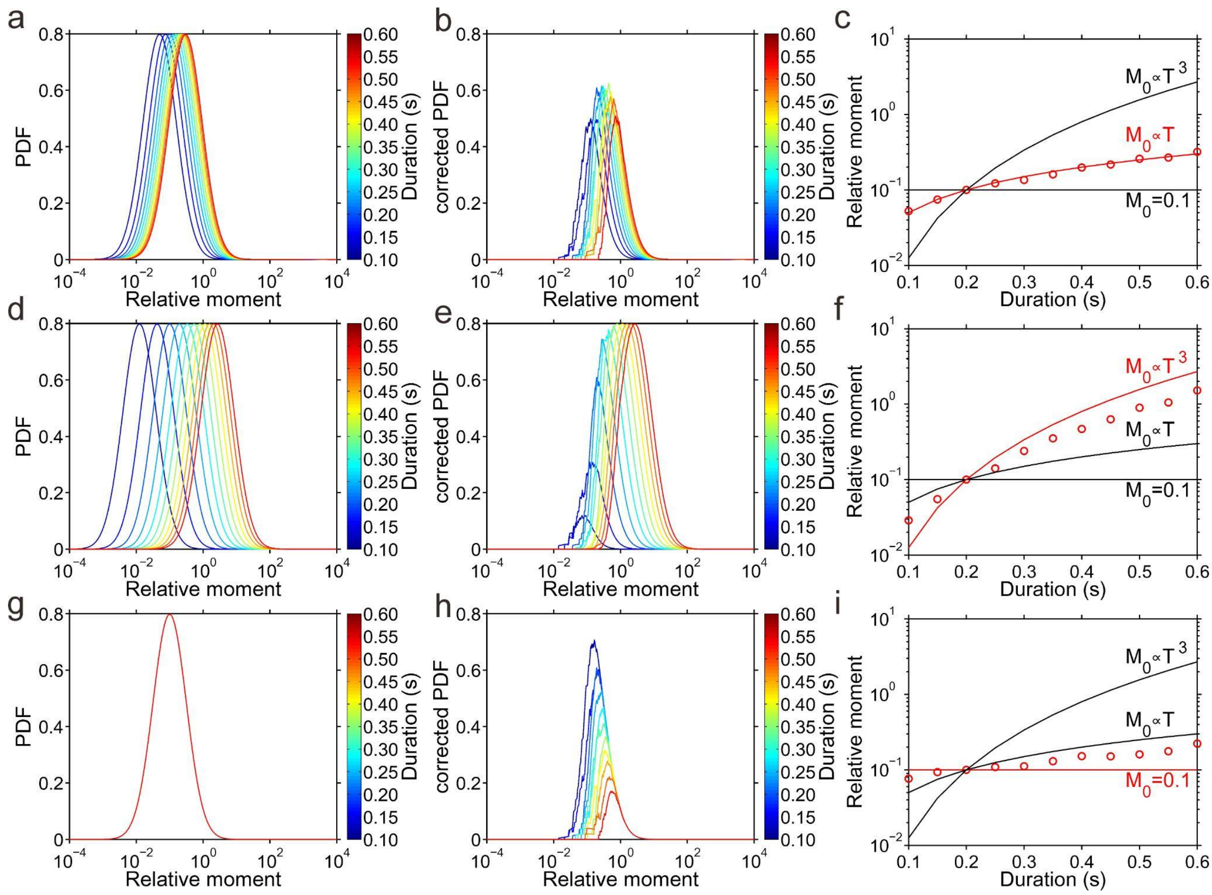

Figure S24. Same as Fig. S22 except that the relative moment at 0.2 sec is set to 0.1.

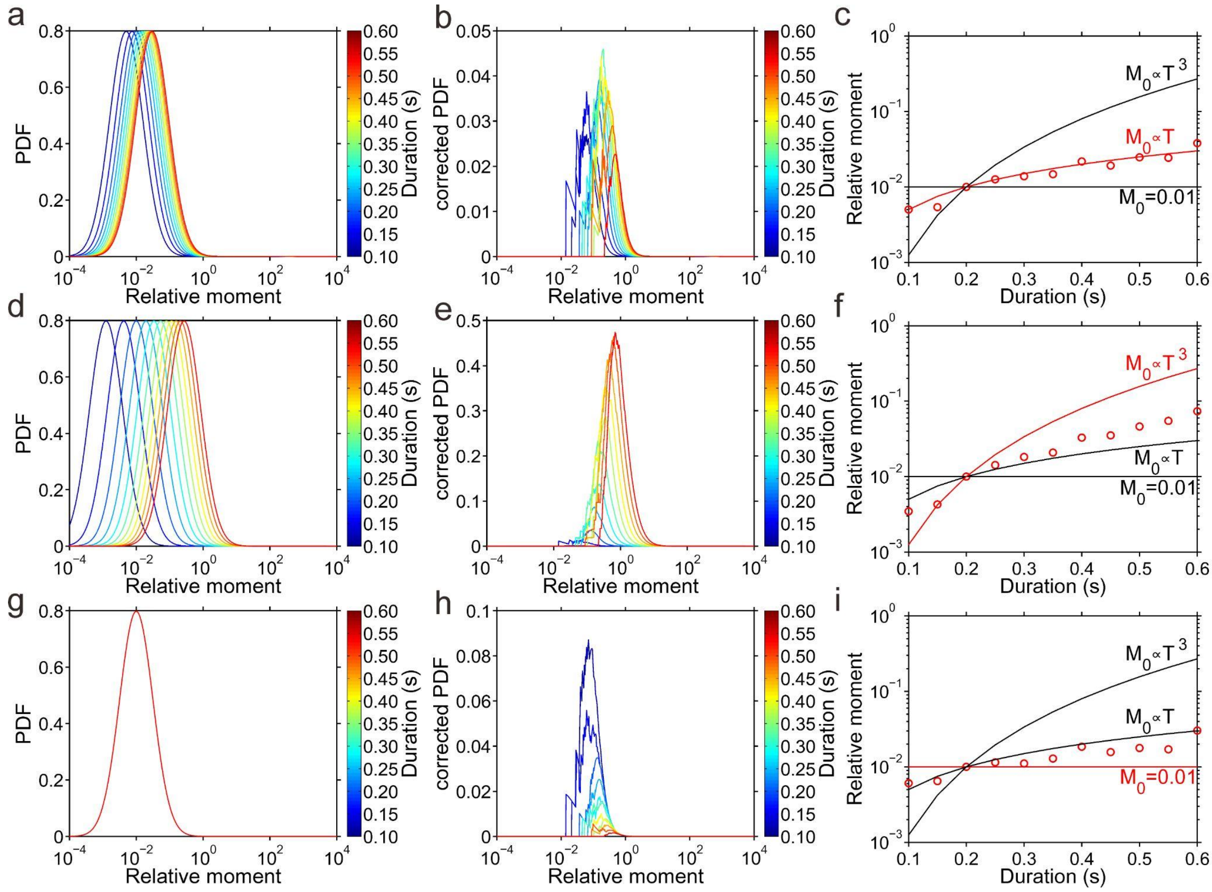

Figure S25. Same as Fig. S22 except that the relative moment at 0.2 sec is set to 0.01.

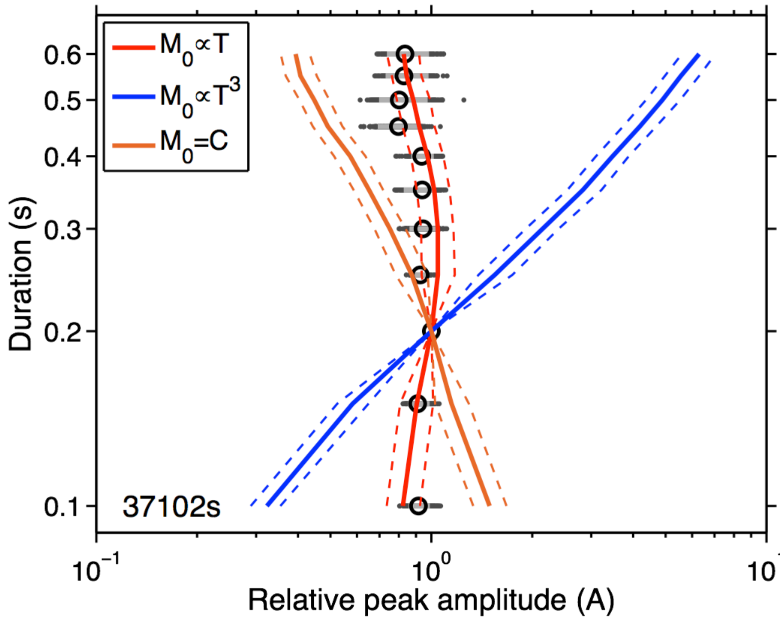

Figure S26. Comparison of the observations of amplitude ratios (family 37102, same as Fig. 4c) with predictions from different moment duration scalings, here assuming the reference moment at 0.2 sec is 0.5 (Fig. S23).

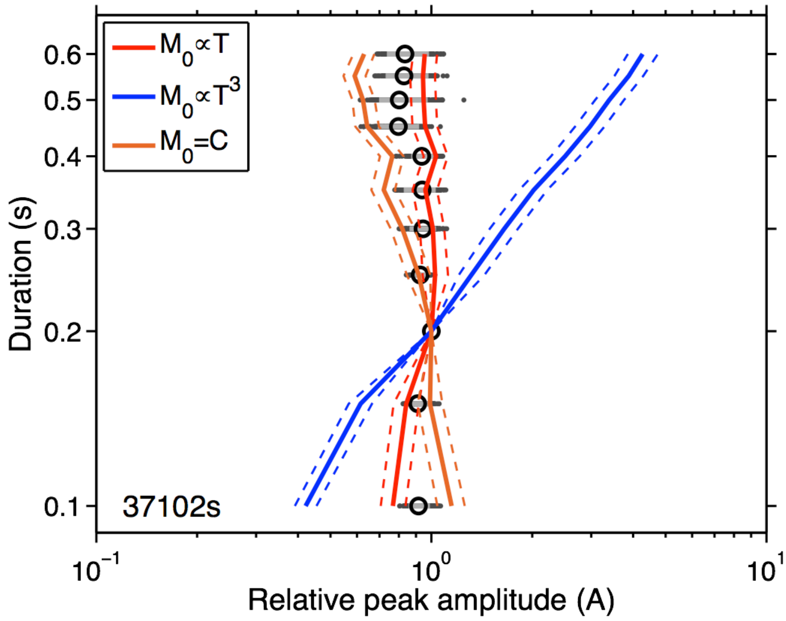

Figure S27. Comparison of the observations of amplitude ratios (family 37102, same as Fig. 4c) with predictions from different moment duration scalings, here assuming the reference moment at 0.2 sec is 0.1 (Fig. S24).

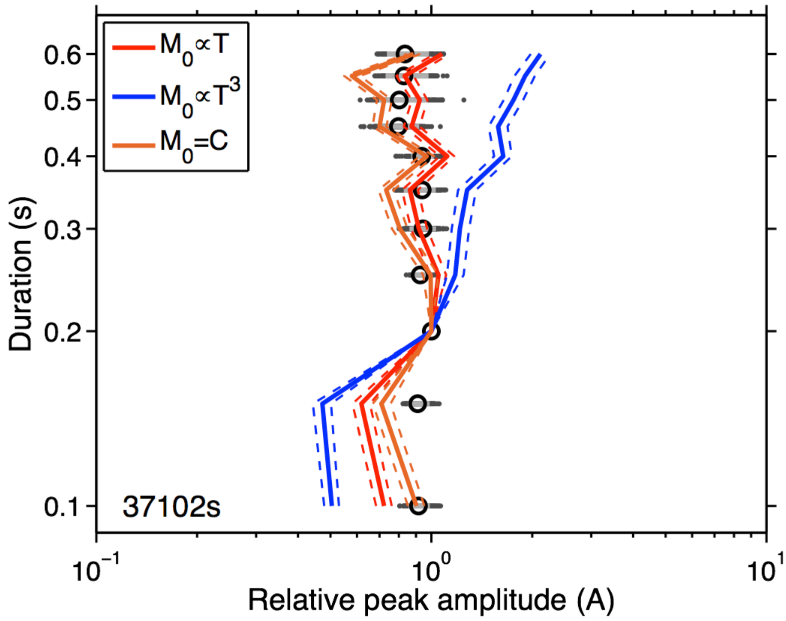

Figure S28. Comparison of the observations of amplitude ratios (family 37102, same as Fig. 4c) with predictions from different moment duration scalings, here assuming the reference moment at 0.2 sec is 0.01 (Fig. S25).

Reference

1. Ide, S., Beroza, G. C., Shelly, D. R., & Uchide, T. (2007). A scaling law for slow earthquakes. *Nature*, *447*(7140), 76-79.
2. Supino, M., Poiata, N., Festa, G., Vilotte, J. P., Satriano, C., & Obara, K. (2020). Self-similarity of low-frequency earthquakes. *Scientific reports*, *10*(1), 1-9.
3. Zhang, J., Gerstoft, P., Shearer, P. M., Yao, H., Vidale, J. E., Houston, H., & Ghosh, A. (2011). Cascadia tremor spectra: Low corner frequencies and earthquake□like high□frequency falloff. *Geochemistry, Geophysics, Geosystems*, *12*(10).